The Astrophysical Journal Letters, 927:L24 (6pp), 2022 March 10 https://doi.org/10.3847/2041-8213/ac589f

H I Gas Playing Hide-and-seek around a Powerful FRI-type Quasar at $z \sim 2.1$

N. Gupta[1], R. Srianand[1], E. Momjian[2], G. Shukla[1], F. Combes[3], J.-K. Krogager[4], P. Noterdaeme[5,6], and P. Petitjean[7]
[1] Inter-University Centre for Astronomy and Astrophysics, Post Bag 4, Ganeshkhind, Pune 411 007, India; ngupta@iucaa.in
[2] National Radio Astronomy Observatory, P.O. Box O, Socorro, NM 87801, USA
[3] Observatoire de Paris, Collège de France, PSL University, Sorbonne University, CNRS, LERMA, Paris, France
[4] Université Lyon1, ENS de Lyon, CNRS, Centre de Recherche Astrophysique de Lyon UMR5574, F-69230 Saint-Genis-Laval, France
[5] Institut d'Astrophysique de Paris, UMR 7095, CNRS-SU, 98bis bd Arago, F-75014 Paris, France
[6] Franco-Chilean Laboratory for Astronomy, IRL 3386, CNRS and Universidad de Chile, Santiago, Chile
[7] Institut d'Astrophysique de Paris, Sorbonne Université and CNRS, 98bis boulevard Arago, F-75014 Paris, France
Received 2022 January 8; revised 2022 February 10; accepted 2022 February 22; published 2022 March 11

Abstract

We present optical spectroscopic and milliarcsecond-scale radio continuum observations of the quasar M1540–1453 ($z_{\rm em} = 2.104 \pm 0.002$) that show associated H I 21 cm absorption at $z_{\rm abs} = 2.1139$. At subkiloparsec scales, the powerful radio source with 1.4 GHz luminosity of 5.9×10^{27} W Hz^{-1} shows Fanaroff–Riley class I morphology caused by the interaction with dense gas within 70 pc of the active galactic nucleus (AGN). Interestingly, while there are indications for the presence of absorption from low-ionization species like Fe II, Si II, and Si III in the optical spectrum, the expected strong damped Lyα absorption is not detected at the redshift of the H I 21 cm absorber. In comparison to typical high-z quasars, the Lyα emission line is much narrower. The "ghostly" nature of the H I Lyα absorber partially covering the broad-line region of extent 0.05 pc and the detection of widespread H I 21 cm absorption covering the diffuse radio source (extent >425 pc) imply the presence of a large clumpy H I halo, which may have been blown by the jet–interstellar medium (ISM) interaction. Further observations are needed to confirm the ghostly nature of the Lyα absorber and obtain a better understanding of the role played by the jet–ISM interaction in shaping the radio morphology of this powerful AGN. The study showcases how joint radio and optical analysis can shed light on the gaseous environment and origin of radio morphology in AGNs at high redshifts, when these are still the assembly sites of giant galaxies.

Unified Astronomy Thesaurus concepts: Active galactic nuclei (16); Radio loud quasars (1349); Radio jets (1347); Quasar absorption line spectroscopy (1317)

1. Introduction

Through the detection of extended Lyα emission, it is now well established that nearly all high-z ($z > 2$) quasars are embedded in low-density warm gas ($T \sim 10^4$ K) halos extending over a few tens to hundreds of kiloparsecs (e.g., Borisova et al. 2016). The spatially resolved distribution and kinematics of this gas exhibit signatures of either infalling or outflowing material, potentially providing evidence for cold accretion flows and active galactic nucleus (AGN) feedback processes (e.g., Arrigoni Battaia et al. 2018; Shukla et al. 2022).

Interestingly, quasar absorption line studies suggest a very low covering factor of the high H I column density (N(H I)) gas around quasars. Specifically, only 2%–5% of the quasars show a damped Lyα system (DLA; with $\log N(\mathrm{H\,I}) \geqslant 10^{20.3}$ cm^{-2}) within ±3000 km s^{-1} of the systemic redshift, $z_{\rm em}$ (referred to as proximate DLAs, or PDLAs; Ellison et al. 2002; Gupta et al. 2021b). The PDLAs associated with AGNs may represent radiation feedback-driven gas outflows and subsequent inflows, i.e., "fountains," within the ionization cone shaped by the torus (e.g., Wada 2012). The leaked radiation from the broad and/or narrow emission line regions (BLRs and/or NLRs) of the quasars can fill the Lyα absorption trough and influence the detectability of such absorbers (Finley et al. 2013). In the case of PDLAs identified through the presence of associated strong metal and H_2 absorption lines, 40%–50% show detectable Lyα emission in the DLA trough, implying that the absorbing cloud only partially covers the BLR (e.g., Fathivavsari et al. 2018; Noterdaeme et al. 2019). In certain cases, hereafter referred to as "ghostly" DLAs, the PDLA close to the central engine is so compact (<1 pc) that the leaked emission completely fills the Lyα trough, and its presence is confirmed only by the detection of the Lyβ absorption line (e.g., Fathivavsari et al. 2017).

Despite their rarity, a complete census and detailed investigations of these absorbers provide crucial insights into the different feedback processes operating in quasar host galaxies (e.g., Noterdaeme et al. 2021a, 2021b). By revealing the chemical composition, clumpiness, and physical conditions in denser and colder phases of the gas at parsec to kiloparsec scales from the nucleus, these absorption line studies can bridge the gap in our understanding of how the ubiquitous halo gas and circumnuclear disk fuel the AGN activity (see Combes et al. 2014; García-Burillo et al. 2019; Storchi-Bergmann & Schnorr-Müller 2019, for examples of nearby AGNs where the central regions are spatially resolvable in emission lines) in distant quasars.

In the radio-loud regime, the H I 21 cm line absorption toward parsec-scale radio jets and extended lobe emission can complement the inherently one-dimensional exploration of optical/ultraviolet absorption line studies (e.g., Adams et al. 2009; Srianand et al. 2015). Further, when the radio source is young, i.e., still embedded within the host galaxy's interstellar medium (ISM), the properties of the ambient medium can also be used to understand the origin of the Fanaroff–Riley class I (FRI; edge-darkened) and II (FRII; edge-brightened) division and evolution of radio jets (e.g., Sutherland & Bicknell 2007; Wagner et al. 2012). The more powerful FRII sources typically have 1.4 GHz

spectral luminosity, $L_{1.4\,\mathrm{GHz}} > 10^{24}$ W Hz^{-1}, while the FRI sources predominantly have lower luminosities. The FRI/FRII dichotomy is among the most debated issues in astrophysics, and it is unclear whether it originates from fundamental differences in the central engine, i.e., black hole spin and accretion mode (Celotti et al. 1997; Ghisellini & Celotti 2001); jet composition (Reynolds et al. 1996); or jet deceleration caused by the ambient clumpy medium (e.g., Bicknell 1995; Mukherjee et al. 2016).

Here we present optical spectroscopy and 1.5 GHz milliarcsecond-scale imaging of a powerful radio quasar, M1540–1453 ($z_{\mathrm{em}} = 2.1$; R.A. = 15:40:15.2353 ± 0.0003; decl. = −14:53:42.409 ± 0.011). The radio source was identified as a high-z quasar through a large optical survey of mid-infrared color-selected powerful radio sources (Gupta et al. 2021a). The associated radio continuum emission corresponds to a 1.4 GHz spectral luminosity, $L_{1.4\,\mathrm{GHz}} = 5.9 \times 10^{27}$ W Hz^{-1}, and radio loudness $R = f_{5\,\mathrm{GHz}}/f_{2500\,\text{Å}} = 4864$). The associated black hole mass (M_{BH}) and Eddington ratio (λ_{Edd}) are $9.2 \times 10^8\ M_\odot$ and 0.08, respectively (Gupta et al. 2021a).

Besides being among the most powerful radio-loud quasars (RLQs) known in the universe (Gupta et al. 2021a), M1540–1453 further stands out for the presence of a cold atomic gas reservoir revealed through the strong H I 21 cm absorption ($N(\mathrm{H\,I}) = (2.06 \pm 0.01) \times 10^{21} \left(\frac{T_s}{100}\right)\left(\frac{1}{f_c}\right)$ cm^{-2} at $z_{21\,\mathrm{cm}} = 2.1139$; Gupta et al. 2021b).[8] Of the total H I 21 cm absorption optical depth, 90% is within $\Delta V_{90} = 167$ km s^{-1}. At $z > 2$, associated H I 21 cm absorption has been detected in only three other cases (Briggs et al. 1993; Moore et al. 1999; Aditya et al. 2021). In general, and based on sensitive low-frequency radio spectroscopic surveys with existing facilities, the powerful quasars at $2 < z < 3.5$ show an extremely small H I 21 cm absorption detection rate ($1.6^{+3.8}_{-1.4}$%; Gupta et al. 2021b). The joint radio and optical investigation of M1540–1453 presented here suggests that, unlike the majority of powerful RLQs, the radio jets in this case exhibit FRI morphology, are interacting with the host galaxy ISM, and are embedded in a H I halo with signatures of infall. Further, the absence of strong H I absorption in the optical spectrum implies a possible ghostly DLA.

Throughout this paper, we use the ΛCDM cosmology with $\Omega_m = 0.315$, $\Omega_\Lambda = 0.685$, and $H_0 = 67.4$ km s^{-1} Mpc^{-1} (Planck Collaboration et al. 2020). At $z = 2.1$, $1'' = 8.5$ kpc.

2. Observations and Data Analysis

2.1. Optical Observations

The optical discovery spectrum of M1540–1453 was obtained on 2015 August 7 using the Robert Stobie Spectrograph on the Southern African Large Telescope (SALT) as part of a large survey of radio-bright (>200 mJy at 1.4 GHz) AGNs (details in Krogager et al. 2018; Gupta et al. 2021a) for the MeerKAT Absorption Line Survey (Gupta et al. 2016). This spectrum covers 4486–7533 Å, that is, only the C IV λ1549 and C III] λ1909 emission lines. The spectral resolution is $R = 1064$ at 6041 Å. As the C IV emission line profile is affected by intrinsic absorption, we use a Gaussian fit to it to estimate the systemic redshift, $z_{\mathrm{em}} = 2.104 \pm 0.002$ (see bottom right panel in Figure 1). This is lower than the redshift, $z_{\mathrm{em}} = 2.113$, we quoted in Gupta et al. (2021b), which was based on the peak of the C IV emission without correcting for the presence of absorption. Note that the peak of the C III] emission line is also affected by absorption.

Intrigued by the detection of a strong H I 21 cm absorption line, we obtained additional SALT spectra on 2021 April 4 and 7 covering the H I Lyα line (see Figure 1). Interestingly, the Lyα emission line from the quasar is weak and narrow, and the expected strong DLA corresponding to the H I 21 cm absorption is absent (see bottom left panel in Figure 1). However, as also mentioned in Gupta et al. (2021b), we detect absorption coincidences at the expected wavelengths of Fe II and Si II (for the latter, see bottom panels of Figure 1). We also detect associated Lyα absorption coincident with C IV absorption lines at $z_{\mathrm{abs}} = 2.0994$, 2.1027, and 2.1180. For $z_{\mathrm{abs}} = 2.1027$, we also detect the N V doublets. For the abovementioned systemic redshift (z_{em}) based on the Gaussian fit to the C IV emission line, these z_{abs} correspond to relative velocities in the range of −450 to +1350 km s^{-1}, and the H I 21 cm absorption peak is redshifted by +950 km s^{-1}. The 1σ uncertainty on z_{em} corresponds to a velocity shift of about ±200 km s^{-1}. This implies that a significant portion of the gas detected in absorption is redshifted, i.e., could be infalling with respect to the quasar. This is subject to the caveat that the C IV emission line is known to underestimate the systemic redshift by several hundred kilometers per second (Richards et al. 2011; Pâris et al. 2012).

2.2. Radio Observations

We observed M1540–1453 with the Very Long Baseline Array (VLBA) of the NRAO on 2021 June 9. A total bandwidth of 256 MHz centered at 1.53 MHz was used. At each of the 10 VLBA stations, eight 32 MHz data channel pairs were recorded using the ROACH Digital Backend and the polyphase filter-bank digital signal-processing algorithm in right- and left-hand circular polarizations and sampled at 2 bits. The data were correlated with the VLBA DiFX correlator (Deller et al. 2011) with 1 s integration time. The observations employed nodding-style phase referencing using the nearby calibrator J1537–1527 with a cycle time of 3.67 minutes. The source 3C 345 was observed as a fringe-finder and bandpass calibrator. The total and on-source observing times were 2.0 and 1.3 hr, respectively. The data editing, calibration, and imaging were done using the Astronomical Image Processing System (AIPS; Greisen 2003). The final image made using Briggs weighting with a robust factor of zero in the AIPS task IMAGR is shown in Figure 2. The restoring beam is 9.0 mas × 3.1 mas with a position angle of +2°.4. The total flux density measured with the VLBA is ∼75 mJy, and the extent of the detected radio emission is ∼50 mas.

3. Results

3.1. Distorted Radio Morphology

In a number of surveys from 100 MHz to 3 GHz, M1540–1453 has been detected as a compact radio source. It has flux densities of 81.4 ± 0.7, 203.3 ± 6.1, 596 ± 13, and 1172.9 ± 13.0 mJy at 3 GHz (Very Large Array Sky Survey, VLASS; Lacy et al. 2020), 1.4 GHz (NRAO VLA Sky Survey, NVSS; Condon et al. 1998), 420 MHz (upgraded Giant Metrewave Telescope, uGMRT; Gupta et al. 2021b), and 170–231 MHz (GaLactic and Extragalactic All-sky MWA Survey, GLEAM, wide; Hurley-Walker et al. 2017), respectively. Among these surveys, the VLASS provides the highest angular resolution. The Gaussian decomposition of the VLASS-detected source implies a deconvolved size of $1''.8 \times 0''.7$ (position angle = 155°). The spectral index between

[8] Here T_s is the spin temperature in Kelvin, and f_c is the covering factor of the H I gas.

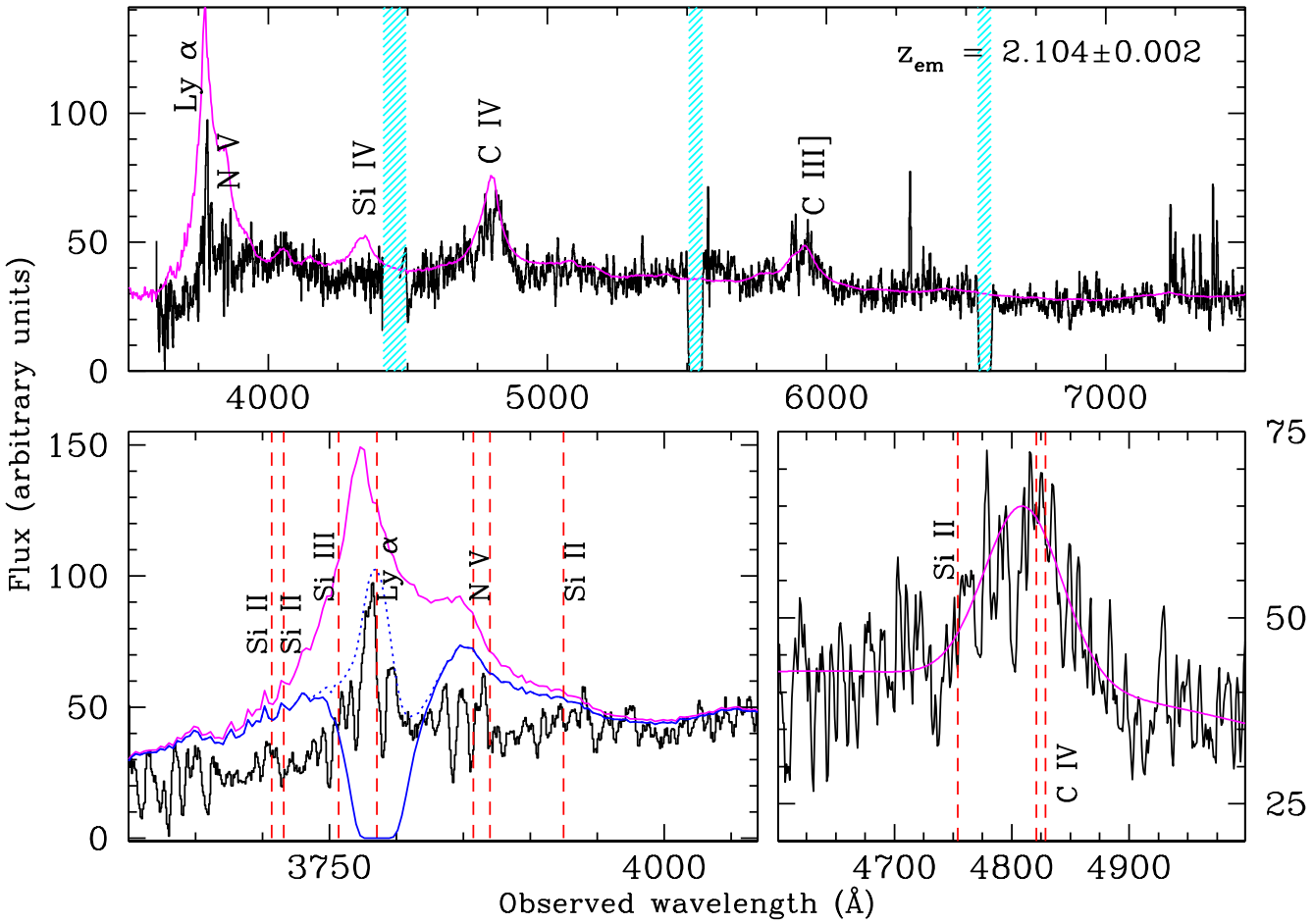

Figure 1. Top: SALT spectrum of M1540–1453 overlaid with the SDSS template spectrum (magenta) of quasars tilted by $\lambda^{0.6}$. The locations of various emission lines are marked, and cyan hashed regions correspond to the CCD gaps. It is evident that while the profiles of the C IV and C III] emission lines roughly follow the template, the Lyα emission is relatively weak and narrow. Bottom left: spectrum around the Lyα emission. The vertical dashed lines show the expected locations of different low-ionization absorption from the H I 21 cm absorber at $z_{\rm abs} = 2.1139$. The solid blue curve is the predicted spectrum if the H I 21 cm absorber (with N(H I) $= 10^{21.3}$ cm^{-2}) completely covers the quasar emission. Bottom right: Gaussian fit (magenta curve) to the C IV profile after masking the absorption line features.

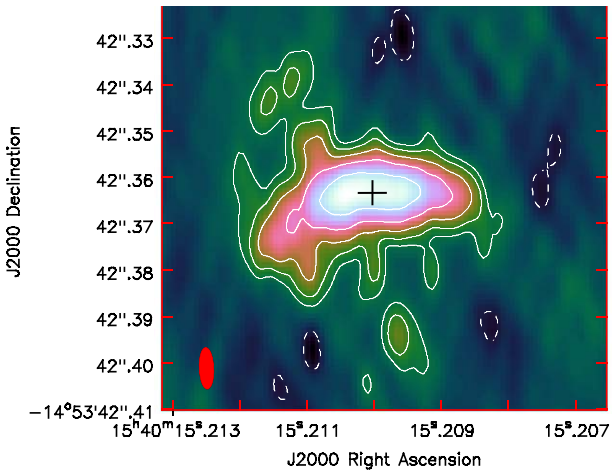

Figure 2. The VLBA 1.53 GHz image of M1540–1453. The rms noise in the image is 65 μJy beam^{-1}. The restoring beam of 9.0 mas × 3.1 mas with a position angle of +2°.4 is shown as an ellipse at the bottom left corner. The contour levels are 250 × (−2, −1, 1, 2, 4, 8, 16, ...) μJy beam^{-1}. The peak intensity is 6.3 mJy beam^{-1}. The plus sign represents the location of the putative radio core/AGN.

the VLASS and NVSS images is $\alpha^{3}_{1.4} = -1.20 \pm 0.05$. At lower frequencies (<1.4 GHz), the GLEAM and uGMRT flux densities imply a slight spectral flattening ($\alpha^{0.42}_{0.2} = -0.91 \pm 0.05$). This may be an indication of a spectral turnover at much lower frequencies (<100 MHz).

The radio source is resolved in our milliarcsecond-scale resolution VLBA image at 1.53 GHz (Figure 2). At this frequency, only ∼41% of the total flux density expected from the NVSS is recovered in the VLBA image. This implies that more diffuse emission, perhaps extending beyond 50 mas (∼425 pc), is associated with the radio source. The extent of the projected radio emission, based on VLASS measurements, could be as large as 10 kpc. It is now well established that at kiloparsec scales, the FRII jets are better collimated than the FRI jets (e.g., Bridle & Perley 1984). Both observations and hydrodynamic simulations suggest that radio jets in both cases are initiated with relativistic speeds, but the deceleration caused by the entrainment of material disrupts the jet and may turn it from an FRII- to FRI-type morphology (e.g., Parma et al. 1987; Bicknell 1995).

In the case of M1540–1453, assuming the plus sign in Figure 2 denotes the location of the radio core, i.e., the AGN, both the eastern and western jets are bright near the base and

gradually fade into diffuse extended emission. No significant brightness asymmetry is observed on either side, but slight bends in the trajectory of the jets at 4 mJy beam^{-1} (fifth contour in Figure 2; ∼8 mas, i.e., ∼70 pc from the core) are noticeable. These are reminiscent of the onset of the dentist-drill effect, beyond which the interaction with the ambient medium makes it harder for the jets to remain collimated and relativistic (Scheuer 1974). Clearly, the radio jet has FRI morphology and is encountering a substantial amount of gas ∼70 pc from the AGN. The similarities in jet morphology on either side of the putative radio core suggest that the ambient media on both sides have similar properties.

By definition, RLQs with the highest radio powers are expected to be of FRII type (e.g., Ghisellini & Celotti 2001). The FRI morphology of M1540–1453 is likely a direct consequence of the jet–ISM interaction. The transition from FRII to FRI morphology due to jet–ISM interaction at subkiloparsec scales has been noticed observationally in one case, i.e., 3C 84 (e.g., Kino et al. 2021), and in numerical simulations with flatter density gradients (Kaiser & Alexander 1997; Wagner et al. 2012).

3.2. Presence of a Ghostly H I Absorber

From the detection of strong H I 21 cm absorption through uGMRT (Gupta et al. 2021b) and the VLBA morphology presented here, the AGN is expected to be buried in a gas-rich environment. In the top panel of Figure 1, we plot the scaled and reddened Sloan Digital Sky Survey (SDSS) QSO template on top of the SALT spectrum. It is evident from the figure that while the profiles of the C IV and C III] emission lines roughly follow the template, the Lyα emission line associated with M1540–1453 is unusually narrow. In the bottom left panel of Figure 1, we zoom in on the Lyα emission and also plot the quasar spectrum modified by an H I absorber with properties based on the 21 cm absorber (i.e., $\log N(\mathrm{H\,I}) = 10^{21.3}$ cm^{-2} at $z_{21\,\mathrm{cm}}$). Here we have assumed $T_s = 100$ K and $f_c = 1$. Clearly, no such absorption is present along the optical sight line toward the AGN.

However, as previously mentioned, the presence of low-ionization gas toward the optical sight line is confirmed through three Fe II absorption features and Si II and Si III absorption lines detected at $z_{21\,\mathrm{cm}}$ (see Figure 1). This may indicate the presence of a ghostly strong Lyα absorption associated with M1540–1453 (Fathivavsari et al. 2017). The key requirement for the presence of a ghostly absorber is that the typical size of the absorbing cloud must be smaller than the BLR but larger than the continuum emitting region at optical/UV wavelengths (Laloux & Petitjean 2021). For M1540–1453, we use $\lambda L_{1350} = 2.4 \times 10^{45}$ erg s^{-1} and Equation (2) of Kaspi et al. (2007) to estimate the BLR radius, $R_{\mathrm{BLR}} = 0.026$ pc. Thus, the absorbing cloud toward the optical sight line ought to be smaller than 0.05 pc (diameter). The detection of damped Lyβ absorption at $z_{21\,\mathrm{cm}}$ is needed to confirm the ghostly nature of this absorber.

4. M1540–1453 and the Ambient Medium

In general, the gas detected in H I 21 cm absorption against a radio source could come from cold atomic gas in a regularly rotating structure, i.e., a circumnuclear disk, or from the host galaxy ISM (e.g., Carilli et al. 1998). In the case of M1540–1453, the diffuse and distorted morphology of the radio emission (extent >425 pc) seen in the 1.53 GHz VLBA image, the broad ($\Delta V_{90} = 167$ km s^{-1}) albeit smooth H I 21 cm absorption profile, and the lack of corresponding DLA in the optical spectrum imply the presence of numerous compact cold gas clouds forming a screen that covers the widespread radio emission and the AGN. With the systemic redshift adopted in this work, the velocities of almost all of the absorbing gas would be consistent with the infall scenario. It can be seen from Figure 10 of Gupta et al. (2021b) that even if the z_{em} coincides with the peak of the H I 21 cm absorption, there is a significant redshifted wing corresponding to infalling cold H I gas.

Using low-frequency flux density estimates from uGMRT and GLEAM and the calibration of Willott et al. (1999), we estimate the kinetic jet power associated with M1540–1453, $P_{\mathrm{jet}} = 3 \times 10^{38}$ $(L_{151}/10^{28}\,\mathrm{W\,Hz^{-1}}) \approx 10^{46}$ erg s^{-1}. This is comparable to the radiative power represented by the bolometric luminosity ($L_{\mathrm{bol}} = 9.1 \times 10^{45}$ erg s^{-1}; Gupta et al. 2021a) of the AGN. Thus, both the kinetic (jet-mode) and radiative (quasar-mode) feedback can affect the ambient gas here. The radiative feedback alone can generate velocities of the order of −445 to +1350 km s^{-1} observed in the optical spectrum (e.g., Faucher-Giguère & Quataert 2012).

Further, the total energy deposited by the radio AGN over its lifetime (10^{6-7} yr) through the interaction with the dense gas amounts to 10^{59-60} erg. In numerical simulations, this is adequate to drive a spherical energy-driven bubble of gas mass with observed velocities (Sutherland & Bicknell 2007). Following this phase, the radio jet drives into the lower-density ISM. The radiatively and kinetically accelerated gas clouds are expected to eventually fall back into the central regions over timescales of tens of megayears (e.g., Wada 2012; Mukherjee et al. 2016). The signatures of infalling gas in the present data are consistent with the above described scenario. Future near-infrared spectroscopy and multifrequency parsec-scale imaging of the radio continuum will provide an accurate systemic redshift measurement and constrain the orientation of the radio source and extent of the H I halo, required to test this model for M1540–1453.

All of the above considerations lead to a scenario summarized in Figure 3. Radio jets are often observed to avoid extended circumnuclear disks, but the jet–disk rotation axis may not be well aligned for a variety of reasons. Instead, the jet axes are often found to be distributed over a wide range of angles within the polar cap (e.g., Verdoes Kleijn & de Zeeuw 2005; Ruffa et al. 2020). In the simplistic case of M1540–1453 presented here, it is assumed that the jet is initially launched along the axis of the inner accretion disk. However, about ∼70 pc from the "core," it gets misaligned due to interaction with the ambient medium. This misalignment and the diffuse nature of radio emission have helped in probing cold gas over a large region, well beyond the initial jet axis. Otherwise, this reservoir, and the presence of a possible ghostly H I absorber in the optical spectrum, would go unnoticed.

A similar scenario has been inferred for the well-studied high-redshift radio galaxy (HzRG) B2 0902+34 at $z \approx 3.39$. The associated radio source, an FRII type in this case, of 5″ (∼40 kpc) extent has an orientation of 30°–45° relative to the observer and is embedded in a huge Lyα halo (extent ∼100 kpc; Lilly 1988; Carilli 1995). The detailed modeling of the detected Lyα halo and H I 21 cm absorption in this case suggests that the radio AGN and the Lyα halo are embedded in an even larger infalling neutral halo of H I mass $>10^{12}$ $M_\odot$

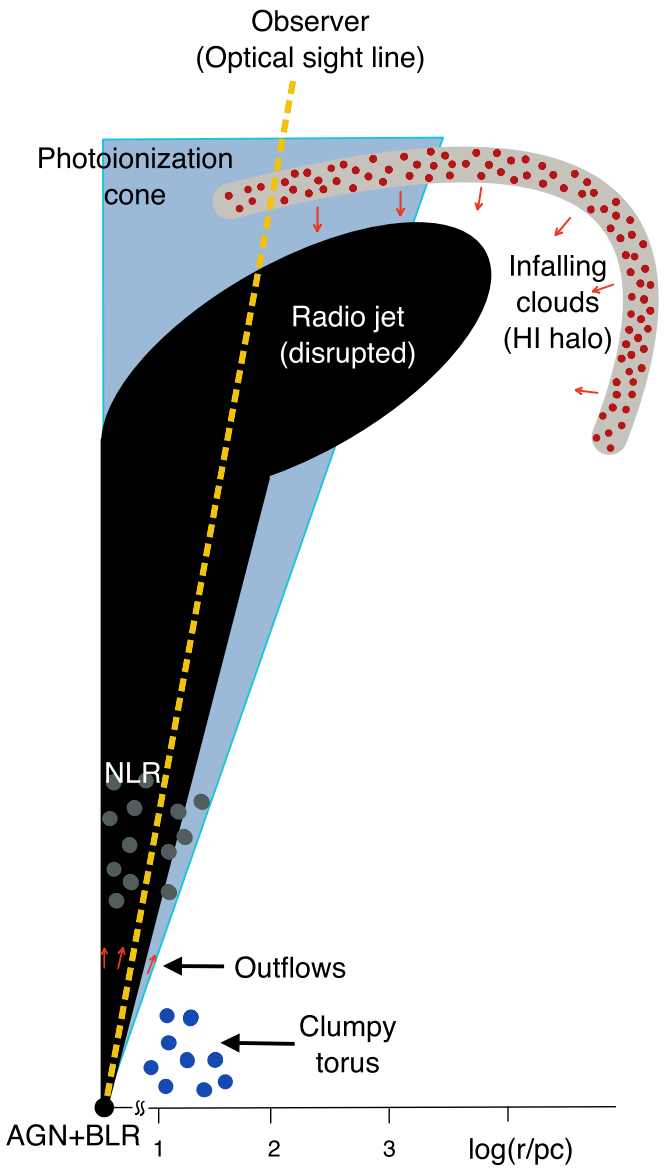

Figure 3. Cartoon depicting a quadrant of M1540–1453 embedded in a clumpy ISM. The quasar's optical sight line (dashed line) may not intercept infalling high-N(H I) clouds. In comparison, extended radio emission (>425 pc) from the lobes will be intercepted by several such clouds, producing the broad redshifted H I 21 cm absorption line. The extent of the H I halo and radio emission could be as large as 10 kpc.

(Adams et al. 2009). Crucial to the infall scenario are the shape of the Lyα profile, the inclination of the radio source, and the redshifts of Lyα emission and H I 21 cm absorption. Despite the relatively large inclination for an HzRG, the central AGN in the case of B2 0902+34 is obscured, suggesting that it has yet to blow out its environment. Object M1540–1453 shows no such obscuration, implying that the AGN feedback has already cleared the obscuring material and blown an H I bubble, which, depending on the accuracy of the systemic redshift, represents infalling material. It is therefore caught at the later stages of evolution. It may also be the case that B2 0902+34 is a protogiant elliptical galaxy in the early phases of evolution, and the collapsing structure represented by the H I shell in this case has an entirely different origin (Adams et al. 2009).

5. Concluding Remarks

At low-z ($z < 0.3$), FRI-type radio sources are typically associated with low-excitation radio galaxies (LERGs) exhibiting low accretion rates ($\lambda_{\rm Edd} < 0.01$) and radio power ($L_{1.4\ \rm GHz} < 10^{25}$ W Hz^{-1}) and hosted by red, massive early-type galaxies ($M_* \geqslant 10^{11}$ $M_\odot$; Best & Heckman 2012). In comparison, M1540–1453 is among the most powerful radio sources ($L_{1.4\ \rm GHz} = 5.9 \times 10^{27}$ W Hz^{-1}) and shows high-excitation optical spectra and efficiently accreting matter ($\lambda_{\rm Edd} = 0.08$). Indeed, the investigation of Best & Heckman (2012) shows that at $L_{1.4\ \rm GHz} = 10^{26}$ W Hz^{-1}, LERGs may be as prominent as high-excitation radio galaxies. Object M1540–1453 emphasizes jet–ISM interaction at subkiloparsec scales as a pathway to produce FRI-type morphology and may be more prevalent at high redshifts ($z \geqslant 2$), when these are still the assembly sites of giant galaxies.

Finally, we note that H I 21 cm absorption detections in AGNs similar to M1540–1453 are rare (Gupta et al. 2021b). Further work is needed to understand the curious case of the AGN presented here. Does it represent a very short phase in the evolution of AGNs or simply a geometrical coincidence? The answers may lead to a better understanding of the subkiloparsec-scale environments through which FRI/FRII jets associated with powerful AGNs are evolving at high z.

We thank the anonymous referee for useful comments and suggestions. This work is based on observations made with SALT and VLBA. The National Radio Astronomy Observatory is a facility of the National Science Foundation operated under cooperative agreement by Associated Universities, Inc.

Facilities: SALT, VLBA.

Software: AIPS (Greisen 2003).

ORCID iDs

N. Gupta https://orcid.org/0000-0001-7547-4241
R. Srianand https://orcid.org/0000-0002-9062-1921
E. Momjian https://orcid.org/0000-0003-3168-5922
F. Combes https://orcid.org/0000-0003-2658-7893
J.-K. Krogager https://orcid.org/0000-0002-4912-9388
P. Noterdaeme https://orcid.org/0000-0002-5777-1629

References

Adams, J. J., Hill, G. J., & MacQueen, P. J. 2009, ApJ, 694, 314
Aditya, J. N. H. S., Jorgenson, R., Joshi, V., et al. 2021, MNRAS, 500, 998
Arrigoni Battaia, F., Prochaska, J. X., Hennawi, J. F., et al. 2018, MNRAS, 473, 3907
Best, P. N., & Heckman, T. M. 2012, MNRAS, 421, 1569
Bicknell, G. V. 1995, ApJS, 101, 29
Borisova, E., Cantalupo, S., Lilly, S. J., et al. 2016, ApJ, 831, 39
Bridle, A. H., & Perley, R. A. 1984, ARA&A, 22, 319
Briggs, F. H., Sorar, E., & Taramopoulos, A. 1993, ApJL, 415, L99
Carilli, C. L. 1995, A&A, 298, 77
Carilli, C. L., Wrobel, J. M., & Ulvestad, J. S. 1998, AJ, 115, 928
Celotti, A., Padovani, P., & Ghisellini, G. 1997, MNRAS, 286, 415
Combes, F., García-Burillo, S., Casasola, V., et al. 2014, A&A, 565, A97
Condon, J. J., Cotton, W. D., Greisen, E. W., et al. 1998, AJ, 115, 1693
Deller, A. T., Brisken, W. F., Phillips, C. J., et al. 2011, PASP, 123, 275
Ellison, S. L., Yan, L., Hook, I. M., et al. 2002, A&A, 383, 91
Fathivavsari, H., Petitjean, P., Jamialahmadi, N., et al. 2018, MNRAS, 477, 5625
Fathivavsari, H., Petitjean, P., Zou, S., et al. 2017, MNRAS, 466, L58
Faucher-Giguère, C.-A., & Quataert, E. 2012, MNRAS, 425, 605
Finley, H., Petitjean, P., Pâris, I., et al. 2013, A&A, 558, A111
García-Burillo, S., Combes, F., Ramos Almeida, C., et al. 2019, A&A, 632, A61

Ghisellini, G., & Celotti, A. 2001, A&A, 379, L1
Greisen, E. W. 2003, in AIPS, the VLA, and the VLBA, ed. A. Heck, 285 (Dordrecht: Kluwer), 109
Gupta, N., Shukla, G., Srianand, R., et al. 2021a, arXiv:2107.09705
Gupta, N., Srianand, R., Baan, W., et al. 2016, in Proceedings of MeerKAT Science: On the Pathway to the SKA, The MeerKAT Absorption Line Survey (MALS) (Trieste: SISSA), 14
Gupta, N., Srianand, R., Shukla, G., et al. 2021b, ApJS, 255, 28
Hurley-Walker, N., Callingham, J. R., Hancock, P. J., et al. 2017, MNRAS, 464, 1146
Kaiser, C. R., & Alexander, P. 1997, MNRAS, 286, 215
Kaspi, S., Brandt, W. N., Maoz, D., et al. 2007, ApJ, 659, 997
Kino, M., Niinuma, K., Kawakatu, N., et al. 2021, ApJL, 920, L24
Krogager, J. K., Gupta, N., Noterdaeme, P., et al. 2018, ApJS, 235, 10
Lacy, M., Baum, S. A., Chandler, C. J., et al. 2020, PASP, 132, 035001
Laloux, B., & Petitjean, P. 2021, MNRAS, 502, 3855
Lilly, S. J. 1988, ApJ, 333, 161
Moore, C. B., Carilli, C. L., & Menten, K. M. 1999, ApJL, 510, L87
Mukherjee, D., Bicknell, G. V., Sutherland, R., & Wagner, A. 2016, MNRAS, 461, 967
Noterdaeme, P., Balashev, S., Combes, F., et al. 2021a, A&A, 651, A17
Noterdaeme, P., Balashev, S., Krogager, J. K., et al. 2019, A&A, 627, A32
Noterdaeme, P., Balashev, S., Krogager, J. K., et al. 2021b, A&A, 646, A108
Pâris, I., Petitjean, P., Aubourg, É., et al. 2012, A&A, 548, A66
Parma, P., Fanti, C., Fanti, R., Morganti, R., & de Ruiter, H. R. 1987, A&A, 181, 244
Planck Collaboration, Aghanim, N., Akrami, Y., et al. 2020, A&A, 641, A6
Reynolds, C. S., Fabian, A. C., Celotti, A., & Rees, M. J. 1996, MNRAS, 283, 873
Richards, G. T., Kruczek, N. E., Gallagher, S. C., et al. 2011, AJ, 141, 167
Ruffa, I., Laing, R. A., Prandoni, I., et al. 2020, MNRAS, 499, 5719
Scheuer, P. A. G. 1974, MNRAS, 166, 513
Shukla, G., Srianand, R., Gupta, N., et al. 2022, MNRAS, 510, 786
Srianand, R., Gupta, N., Momjian, E., & Vivek, M. 2015, MNRAS, 451, 917
Storchi-Bergmann, T., & Schnorr-Müller, A. 2019, NatAs, 3, 48
Sutherland, R. S., & Bicknell, G. V. 2007, ApJS, 173, 37
Verdoes Kleijn, G. A., & de Zeeuw, P. T. 2005, A&A, 435, 43
Wada, K. 2012, ApJ, 758, 66
Wagner, A. Y., Bicknell, G. V., & Umemura, M. 2012, ApJ, 757, 136
Willott, C. J., Rawlings, S., Blundell, K. M., & Lacy, M. 1999, MNRAS, 309, 1017